AIAA JOURNAL
Vol. 36, No. 9, September 1998

Modeling Flow and Heat Transfer in Vortex Burners

Anatoly Borissov,* Vladimir Shtern,† and Fazle Hussain‡
University of Houston, Houston, Texas 77204-4792

A powerful approach is developed to predict and optimize flow pattern and to improve heat and mass transfer in vortex burners. New analytical solutions of the Navier–Stokes, heat, and diffusion equations are obtained, and the technique of matching asymptotic expansions is developed. This allows us to describe complex swirling flows with recirculation zones and three-dimensional fields of temperature and concentration. This approach helps in deducing the appropriate flow pattern, shape and position of a flame front, heat transfer, and geometry of the vortex burner. Optimal parameters are found for flame stabilization and flame-surface expansion, prolonging the residence time of the reactants favorable for complete combustion. This approach greatly facilitates finding the optimum because it is much less laborious than computational fluid dynamics methods and allows a wider parametric search.

Nomenclature

i	$= \sqrt{-1}$
k	= coefficient of thermal diffusion
m	= normal mode number
$\boldsymbol{r}$	= radius vector
r_e	= radius of external cylindrical surface
r_0	= radius of vortex core, radius of internal cylindrical surface
s	= coordinate along streamline
T	= temperature
$T_0(z^*)$	= instant temperature distribution along the axial coordinate
$T_1(t, z)$	= ξ- and ϕ-independent temperature; Eq. (7)
$T_2(\xi, \phi)$	= t- and z-independent temperature; Eq. (7)
t	= time
$\boldsymbol{v}$	= velocity vector
x, y, z	= orthogonal coordinates
$y_e(x)$	= analytical function for Landau jet exact solution
$Z(r)$	= function of axisymmetric flame surface
z^*	= integration coordinate
Γ	= circulation
ΔT	= dimensionless temperature difference
η	= boundary-layer thickness
ν	= kinematic viscosity
ξ	= logarithmic radius
ρ	= density
Ψ, ψ	= dimensional and dimensionless stream function

Subscripts

e	= external surface
r, ϕ, z	= radial, tangential, axial derivatives for temperature and concentration
t	= time derivative
ξ	= logarithmic radius derivative
0	= inner surface
∞	= ambient conditions

Superscript

*	= virtual coordinate

Presented as Paper 97-1998 at the AIAA 28th Fluid Dynamics Conference, Snowmass Village, CO, June 29–July 2, 1997; received Aug. 8, 1997; revision received March 18, 1998; accepted for publication May 4, 1998.

*Research Scientist, Department of Mechanical Engineering; currently Director, Research and Development, Equadyne International, 240 E. Barbours Cut Boulevard, La Porte, TX 77571.

†Research Associate Professor, Department of Mechanical Engineering. Member AIAA.

‡Professor, Department of Mechanical Engineering. Associate Fellow AIAA.

I. Introduction

PREDICTION and control of combustion in vortex burners have serious inherent difficulties. The major difficulty is that swirling flows are typically complicated, containing recirculatory domains. Also, the flows have features difficult to predict such as collapse,[1] i.e., strong concentration of the axial and angular momenta; bistability,[2] i.e., two stable states for the same values of control parameters; the Ranque effect,[3] thermal separation; and vortex breakdown.[4] In this paper, we develop a new powerful approach to study complex flows and, in particular, the velocity, temperature, and concentration fields in vortex burners. Our approach is based on newly found analytical solutions of the governing equations. The key point is the generalization of the irrotational vortex sink to incorporate a vortical axial flow.

The planar vortex-sink or vortex-source flow is one of the simplest solutions of the Euler (and Navier–Stokes) equations. Such solutions (especially point vortices) are widely used as building blocks for modeling more complex practical flows.[4] Incorporating the axial flow significantly enhances modeling abilities. However, previous analytical solutions combining the sink and axial flows do not involve swirl. They describe flows near an infinite porous cylinder and in a porous annulus[5] and, thus, address very specific flows of limited practical interest. In contrast, our solution addresses swirling flows of widespread technological importance. Wang's review[5] and our extensive literature search revealed no other works in this subject.

The vortex-sink relation for the radial and azimuthal velocities is a common feature of many swirling flows. This essentially follows from 1) conservation of angular momentum in regions where viscous diffusion is negligible and 2) entrainment of ambient fluid by near-axis jet-like flows. The jet axis serves as a line sink for entrainment flows, as shown by Schlichting[6] for swirl-free jets and by Long[7] for swirling jets.

The vortex-sink region is observed not only in open but also in confined swirling flows. Far from boundaries, a flow is typically oblivious of most of the constraint posed by boundary conditions. For instance, flows in vortex tubes[8] and vortex generators[9] are strongly asymmetric near tangential inlet nozzles but become nearly axisymmetric even at downstream distances comparable with the nozzle diameter. Also, outside the boundary layer, the no-slip condition on sidewalls does not influence the main flow of interest. For these reasons, the fine details of boundary conditions can be reasonably omitted for studying robust features of swirling flows, as undertaken here.

The values of certain parameters (governed by conservation laws) are crucial for large-scale flow patterns. These parameters include the entrainment rate (here the radial Reynolds number Re) and circulation (the swirl Reynolds number Γ). Such a reduction of detailed boundary conditions to a few integral characteristics is consistent with the fact that the vortex-sink region is observed in a wide variety of swirling flows. Using Reynolds number Re and Γ for the radial and swirl flows, we show that only three more parameters are required to specify the axial velocity.

A further extension is to use the generalized vortex sink as an outer solution and to match with inner solutions, e.g., with the axisymmetric Schlichting and swirling jets, to remove the vortex-sink singularity on the axis. This enables modeling of internal, i.e., away from walls, separation, which is a rather subtle but common phenomenon in swirling flows. Such separation causes the appearance of recirculatory domains, which are either semi-infinite or compact (bubble- and torus-shaped) regions. The recirculatory domains are essential features of vortex combustion, vortex breakdown, and the Ranque effect.

Based on the generalized vortex sink, we obtain new analytical solutions for the heat and diffusion equations. These solutions help in describing the three-dimensional distributions of temperature and concentration observed in vortex burners.

Because practical flows are almost always turbulent, their modeling includes interpretation of the kinematic viscosity as the uniform eddy viscosity. Such models are found to be satisfactory in describing the mean velocity fields of turbulent jet-like and swirling flows.[6,10,11] The interpretation of the diffusion coefficients for heat and concentration is similar to that of the eddy viscosity.

II. Generalized Vortex Sink

We consider a steady axisymmetric swirling flow, where v_r, v_ϕ, and v_z are the velocity components in cylindrical coordinates (r, ϕ, z) (Ref. 12). The new solution of the Navier–Stokes equations for a viscous incompressible fluid is[13]

$$v_r = Re\nu/r \tag{1a}$$

$$v_\phi = \Gamma\nu/r \tag{1b}$$

$$v_z = \left[W_c + W_p(r/r_0)^2 + W_r(r/r_0)^{Re}\right]\nu/r_0 \tag{1c}$$

$$p = p_\infty - \tfrac{1}{2}\rho(\nu/r)^2(Re^2 + \Gamma^2) + \rho(\nu/r_0)^2 Pz/r_0 \tag{1d}$$

where p is pressure, $P = r_0^3(\rho\nu^2)^{-1}\partial p/\partial z$ is a dimensionless parameter characterizing the axial pressure gradient, and $W_p = P/(4 - 2Re)$. The dimensionless constants in Eq. (1c) characterize contributions to the axial flow from the uniform stream W_c, the axial pressure gradient W_p, and entrainment, i.e., the effect of the radial flow, W_r. The (v_r, v_ϕ) flow is the well-known vortex sink (vortex source) for $Re < 0$ ($Re > 0$), whereas solution (1c) for v_z is new.

The streamline equation $d\boldsymbol{r}/ds = \boldsymbol{v}$ is explicitly integrated to yield

$$z/r_0 = z_0/r_0 + a(r/r_0)^2 + b(r/r_0)^{Re+2} + c(r/r_0)^4 \tag{2a}$$

$$\phi = \phi_0 + S\,\ln(r/r_0) \tag{2b}$$

where $a = W_c(2Re)^{-1}$, $b = W_r[Re(Re+2)]^{-1}$, $c = W_p(4Re)^{-1}$, and the swirl parameter $S = v_\phi/v_r = \Gamma/Re$. This parameter naturally appears in the theory, but S is convenient also for comparison with practical flows. For example, S can be easily calculated for vortex chambers, vortex tubes, and burners, where both the radial velocity and circulation are determined by the geometry of guide vanes and flow rate. Using the composite solutions (Secs. VI and VII), one can calculate other swirl numbers, e.g., based on the angular and axial momenta, which are used to treat experimental data.

The velocity field is identical on axisymmetric stream surfaces [Eq. (2a)] differing only by a shift (z_0) along z. Streamlines curve around on these surfaces, and their projection on $z = \text{const}$ planes are logarithmic spirals [Eq. (2b)]. The planar vortex sink is a particular case corresponding to $a = b = c = 0$ in Eq. (2).

To visualize flow patterns for comparison with experiments, it is convenient to use the Stokes stream function Ψ, i.e., $v_r = -r^{-1}\partial\Psi/\partial z$ and $v_z = r^{-1}\partial\Psi/\partial r$. The dimensionless stream function $\psi = \Psi(\nu r_0 Re)^{-1}$ has the form

$$\psi = a(r/r_0)^2 + b(r/r_0)^{Re+2} + c(r/r_0)^4 - z/r_0 \tag{3}$$

According to Eq. (1c), pressure decreases as $r \to 0$. Inasmuch as typically $\Gamma^2 \gg Re^2$ in practical applications, the pressure drop near the axis is mainly an effect of swirl. In physical terms, this pressure drop reflects the balance between the centrifugal force and the radial pressure gradient. The pressure can also decrease or increase in the axial direction, depending on the sign of P.

Thus, the set of Eqs. (1–3) is a new five-parameter solution family. As the number of parameters is quite large, the solution can capture a wide variety of nontrivial flow patterns. Relevant adjustment of the parameters enables one to approximate, with relative ease, some important elements of practical flows.

III. Two-Dimensional Solutions of the Heat Equation

The equation for convective heat transfer in cylindrical coordinates,

$$T_t + v_z T_z + v_r T_r + v_\phi/r\,T_\phi = k\left[r^{-1}(rT_r)_r + r^{-2}T_{\phi\phi} + T_{zz}\right]$$

is reduced to

$$r^2(T_t + WT_z - T_{zz}/Pr) + ReT_\xi + \Gamma T_\phi = (T_{\xi\xi} + T_{\phi\phi})/Pr \tag{4a}$$

by using Eq. (1), $\xi = \ln(r/r_0)$, and multiplying by r^2/ν. Here subscripts denote the differentiation; $Pr = \nu/k$ is the Prandtl number; $W = v_z r_0/\nu$, $Re = v_r r/\nu$, and $\Gamma = v_\phi r/\nu$ are constants; and W is from Eq. (1c). If the temperature field is steady and z independent, then one has the equation with constant coefficients,

$$ReT_\xi + \Gamma T_\phi = Pr^{-1}(T_{\xi\xi} + T_{\phi\phi}) \tag{4b}$$

which has the normal-mode solutions,

$$T = \exp(\alpha\xi + im\phi) \tag{4c}$$

where $\alpha = \alpha_1$ or α_2, which are roots of the dispersion relation $\alpha^2 - \alpha Pe - m^2 - im\Gamma_p = 0$, and $Pe = Pr\,Re$ and $\Gamma_p = Pr\,\Gamma$ are the Peclet numbers based on the radial and swirl velocities. A general solution of Eq. (4b) is obtained by the superposition of the normal modes (4c), whose coefficients can be determined from boundary conditions.

A. Axisymmetric Solution

In particular, the axisymmetric solution of Eq. (4b) is

$$T = T_c + T_r(r/r_0)^{Pe}$$

where T_c and T_r are constants. In the context of this paper, the cases $Pe = -4Pr$ and $-Pr$ are of special interest for matching with the inner solutions (see Sec. VI.B). For $Pe < 0$, $T_c = T_\infty$ is an ambient temperature (given at $r = \infty$) and $T_r = T_0 - T_c$, where T_0 is the temperature at $r = r_0$. One can interpret T_0 as the temperature of a porous cylinder, which models a near-axis core. Thus, there are the two relevant solutions

$$T = T_\infty + (T_0 - T_c)(r/r_0)^{-4Pr} \tag{5a}$$

$$T = T_\infty + (T_0 - T_c)(r/r_0)^{-Pr} \tag{5b}$$

Swirl does not influence the axisymmetric temperature field, but its influence is crucial in a nonaxisymmetric heat problem. The exponents α_1 and α_2 are complex for m and $\Gamma_p \neq 0$, which means that there are temperature oscillations in the r direction. This is a specific effect of swirl, which is of importance for combustion applications, where isothermal surfaces, e.g., the flame front, become more extended and bent, increasing heat and mass transfer fluxes and thus improving the combustion efficiency.

B. Nonaxisymmetric Solution

Consider the particular problem in which there is a uniform temperature gradient (stratification) on the boundary $r = r_e$ of the external cylinder and there is no heat flux at the boundary $r = r_0$ of the internal cylinder. The boundary conditions are $T = \sin\phi$ at $r = r_e$ and $\partial T/\partial r = 0$ at $r = r_0$, where temperature T is normalized to its

amplitude value. The solution of Eq. (4b) is a superposition of the normal modes with $m = \pm 1$,

$$T = \text{real}\Big\{c_1\big(a_2 r^{a1} - a_1 r^{a2}\big)[i\cos(\phi) - \sin(\phi)] + c_2\big(a_4 r^{a3} - a_3 r^{a4}\big)[i\cos(\phi) + \sin(\phi)]\Big\} \tag{5c}$$

where the coefficients are given by

$$a_1 = Pe/2 + [p_2 + i\Gamma]^{\frac{1}{2}}, \qquad a_2 = Pe/2 - [p_2 + i\Gamma]^{\frac{1}{2}}$$

$$a_3 = Pe/2 + [p_2 - i\Gamma]^{\frac{1}{2}}, \qquad a_4 = Pe/2 - [p_2 - i\Gamma]^{\frac{1}{2}}$$

$$c_1 = \frac{0.5}{a_1 r_e^{a2} - a_2 r_e^{a1}}, \qquad c_2 = \frac{0.5}{a_4 r_e^{a3} - a_3 r_e^{a4}}$$

$$p_2 = Pe^2/4 + 1$$

Figure 1a shows the isotherms according to Eq. (5c) in the section $z = \text{const}$ at $\Gamma = 50$, $Re = -4$, $Pr = 1$, $r_e = 5$, and $r_0 = 1$. The curve $T = 0.8$ is the boundary of the hottest (brightest) near-wall region, and the curve $T = -0.8$ is the boundary of the coldest (darkest) near-wall region. The mesh is $\Delta T = 0.4$. The curves start and finish on the outer wall, except the two curves $T = 0$, which start at $\{x = \pm 5, y = 0\}$ and finish on the inner wall. Without conduction, T would be constant along the stream surfaces, and the curves in Fig. 1a would become logarithmic spirals. Heat diffusion across streamlines tends to make temperature uniform ($T = 0$) as r decreases. As a result, the curves $T = \text{const} \neq 0$ terminate at some r as shown in Fig. 1a.

Figure 1b shows a three-dimensional view of the surface $T(x, y)$. One can see the ridge and valley corresponding to the maximum and minimum of T with respect to r for a fixed ϕ. These extrema are located on spiral curves that start at $\{x = 0, y = \pm 5\}$ and finish on the inner cylinder surface. If $r_0 \to 0$, the temperature distribution is similar to that shown in Fig. 1a. The curves $T = 0$ are logarithmic spirals extending up to the origin, but other curves terminate at nonzero values of r. Thus, the temperature is nearly uniform and equal to zero in the vicinity of the origin.

In the still fluid, the solution is $T = (r/r_e)\sin\phi$, and therefore, the isotherms would be horizontal lines in Fig. 1a. The vortex-sink flow significantly increases the isothermal-surface area between the cylinders and, therefore, increases heat transfer. For combustion applications, region $T > 0$ and surface $T = 0$ can be viewed as the flame region and flame front, respectively. The flame plume in Fig. 1a is the bright region between the curves $T = 0$. Increasing plume surface makes combustion more effective and allows remarkable reduction in the volume of a combustion chamber; this serves as a major advantage of vortex furnaces.

IV. Solution of the Diffusion Equation

For combustion applications, one needs also a solution of the diffusion equation. Let C be the concentration of a gaseous fuel. If C is small in comparison with an oxidizer concentration, then the reaction-diffusion equation is linear:

$$Ps\,C_\xi + \Gamma s\,C_\phi = C_{\xi\xi} + C_{\phi\phi} - DaC \tag{6}$$

where $Ps = ScRe$, $\Gamma s = Sc\Gamma$, where Sc is the Schmidt number, and Da is the Damköhler number, which is the diffusion/kinetic time ratio for a chemical reaction. The last term in Eq. (6) describes the fuel consumption (sink) due to combustion. As Eq. (4), Eq. (6) has the normal-mode solutions

$$C = \exp(\alpha\xi + im\phi)$$

where $\alpha = \alpha_1$ or α_2, which are roots of the dispersion relation $\alpha^2 - \alpha Ps - m^2 - im\Gamma s - Da = 0$. Figure 2a shows the results for the boundary conditions $C = (1 - \sin\phi)/2$ at $r = r_e$ and $\partial C/\partial r = 0$ at $r = r_0$. We take $Sc = 1$ and $Da = 10$ with other parameters remaining the same as in Fig. 1a. The reason for $Da = 10$ is that Eq. (6) can be applied only for the diffusion kind of combustion, where the characteristic time of reaction is significantly smaller than the time of diffusion, i.e., $Da \gg 1$.

Figure 2a shows the contours $C = 0.8$, 0.6, 0.5, 0.4, and 0.2. The isolines of concentration and temperature are similar in Figs. 1a and 2a. However, C is small where T is large and vice versa because the superposition of the concentration and temperature with appropriate coefficients is enthalpy, which is nearly uniform along streamlines for high Reynolds numbers. Figure 2b shows the three-dimensional view of the surface $C(x, y)$. Figures 1b and 2b look similar, but note that the directions of the x and y axes are opposite.

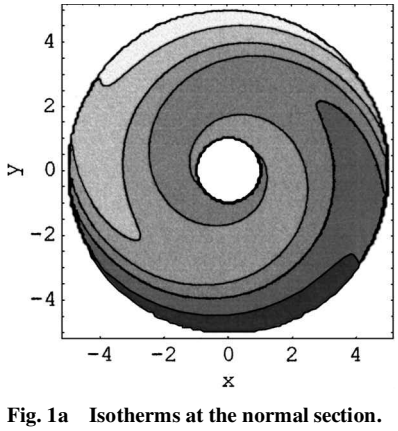

Fig. 1a Isotherms at the normal section.

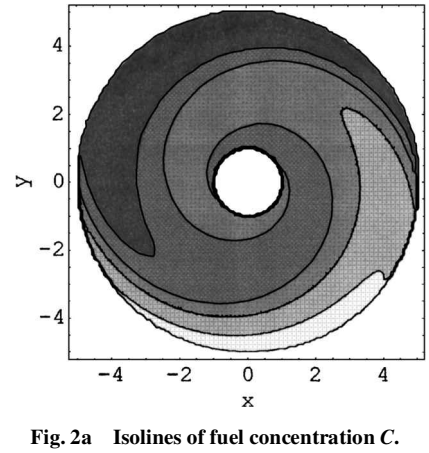

Fig. 2a Isolines of fuel concentration C.

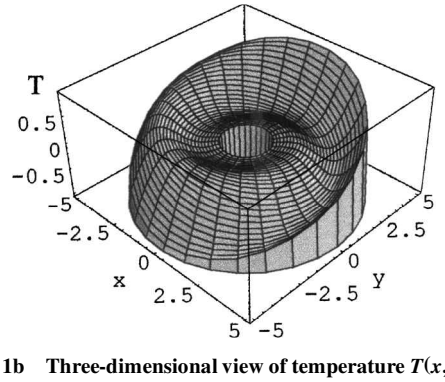

Fig. 1b Three-dimensional view of temperature $T(x, y)$.

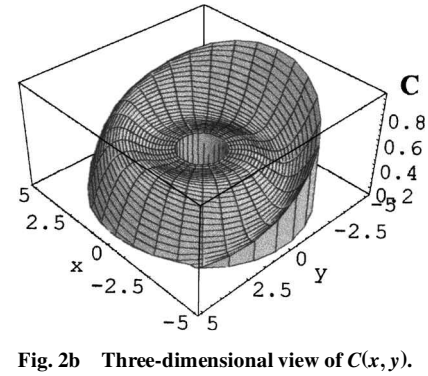

Fig. 2b Three-dimensional view of $C(x, y)$.

V. Three-Dimensional Thermal Solution

The preceding problems are two dimensional, whereas combustion is three dimensional in vortex furnaces. Three-dimensional heat transfer in the generalized vortex-sink flow needs numerical calculation in general. However, an analytical solution is also available for a particular radial distribution of the axial velocity. Following the analytical style of this paper, we now address this particular case. To make the coefficient of T_z in Eq. (4a) constant, one needs W to be constant, which corresponds to uniform flow. This does occur with $W_r = W_p = 0$ in Eq. (1c). Then Eq. (4a) is

$$r^2(T_t + W_c T_z - T_{zz}/Pr) + ReT_\xi + \Gamma T_\phi = (T_{\xi\xi} + T_{\phi\phi})/Pr \quad (7)$$

A solution of Eq. (7) can be found in the form

$$T(t, z, \xi, \phi) = T_1(t, z) + T_2(\xi, \phi)$$

where $T_1(t, z)$ is governed by the equation

$$T_t + W_c T_z - Pr^{-1} T_{zz} = 0$$

whose general solution is a superposition of the normal modes

$$T = C(\gamma)\exp(\gamma z + \lambda t), \qquad \lambda = \gamma^2/Pr - \gamma W_c$$

For the problem with initial condition $T_1(t, z) = T_0(z)$, the solution is

$$T_1(t, z) = \int_{-\infty}^{\infty} T_0(z^*)\exp\left[-Pr\frac{(z - W_c t z^*)^2}{4t}\right] \Big/ \left(\frac{4\pi t}{Pr}\right)^{\frac{1}{2}} dz^*$$

Because $T_2(\xi, \phi)$ is t and z independent, it satisfies Eq. (7) if T_2 satisfies Eq. (4b). Therefore, $T_2(\xi, \phi)$ is a superposition of the normal modes (4c) whose coefficients are specified by boundary conditions. Thus, the general solution is

$$T(t, z, \xi, \phi) = T_1(t, z) + \Sigma C_{\alpha m}\exp(\alpha\xi + im\phi)$$

where the sum is taken with respect to $m = 0, \pm 1, \pm 2, \ldots$, and $\alpha = \alpha_1, \alpha_2$. For a steady problem, the solution reduces to

$$T(z, \xi, \phi) = T_0\exp(PrW_c z) + \Sigma C_{\alpha m}\exp(\alpha\xi + im\phi)$$

Parameters m, T_0, and $C_{\alpha m}$ are specified along with the boundary conditions at $r = r_e$ and r_0.

As an example, consider a model of the temperature field in a vortex furnace, taking

$$T = \frac{1}{2}[1 + \cos(3\phi) + 2\exp(\gamma z)] \qquad \text{at} \qquad r = r_e$$
$$\frac{\partial T}{\partial r} = 0 \qquad \text{at} \qquad r = r_0, \qquad \gamma = PrW_c \quad (8)$$

These boundary conditions correspond to the realistic furnaces where the temperature is nearly uniform near the axis. The temperature distribution on the outer cylinder has three local maxima and minima in the azimuthal direction. The three hot regions, for example $T > 1.9$, model combustion: Typically, there are three or four plumes located at the same height with equal azimuthal distances in vortex furnaces.

To satisfy Eq. (8), the normal modes $m = 0$ and ± 3 are needed. Because there are two eigenvalues for each m, the solution is a superposition of six modes; the calculation of coefficients, being simple but lengthy, is omitted here. Figure 3 shows the results for $Pe = -2$, $\Gamma_p = 50$, $\gamma = 0.2$, $m = 3$, $r_e = 5$, and $r_0 = 1$.

Figure 3a shows the 10 isotherms $T = \text{const}$ in the range $\exp(0.4) \le T \le \exp(0.4) + 1$ with the uniform mesh $\Delta T = \frac{1}{11}$ at $z = 2$. Figure 3b shows the three-dimensional view of the surface $T(x, y, z) = 2$. This surface consists of three separated parts. Each part touches the plane $z = 0$ at a single point, expands upward, and is cut at the height $z = 2$ (to make the figure compact). One can imagine that the regions inside the surface consist of three flame plumes.

The number of analytical solutions for heat and mass transfer based on the preceding approach can be made significantly large. The next stage is to develop this approach with the help of the matching technique. First, we apply this technique to generalize the flowfield.

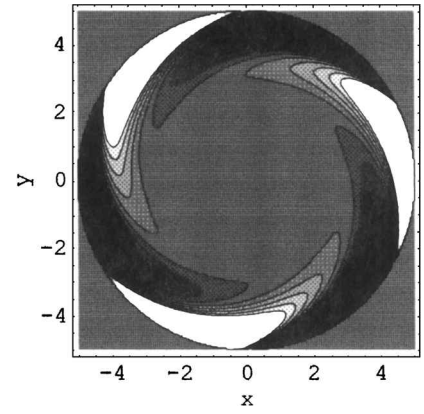

Fig. 3a Isotherms at $z = 2$.

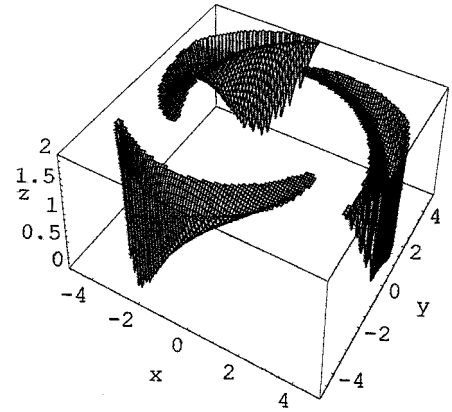

Fig. 3b Surface $T(x, y, z) = 2$ modeling three-plume combustion.

VI. Matched Solutions

A. Matching Technique

Solution (1) having the vortex-sink singularity on the axis can be viewed as an outer part of a more complicated flow. The outer solution (1) and an inner solution describing a jet-like flow near the axis can be matched so as to constitute a composite solution. A general technique of matching asymptotic expansion[14] states that the outer, for example, $y_o(x)$, and the inner, $y_i(\eta)$, solutions satisfying the condition $y_o(0) = y_i(\infty)$ can constitute multiplicative $y_m(x) = y_o(x)y_i(\eta)/y_i(\infty)$ and additive $y_a(x) = y_o(x) + y_i(\eta) - y_i(\infty)$ compositions, where y_m and y_a are uniform approximate solutions. It is supposed here that there is a boundary layer at $x = 0$ and η is a scaled x.

To illustrate how the matching technique works, consider the Landau jet,[12] which is an example closely related to the topic at hand. In terms of the Stokes stream function Ψ, the Landau solution is $\Psi = \nu(r^2 + z^2)^{1/2}y(x)$, where $y = y_e = 2Re_a(1 - x^2)/[4 + Re_a(1 - x)]$ and $x = z/(r^2 + z^2)^{1/2}$. Here, Re_a is the Reynolds number based on the axial velocity at $x = 1$.

As $Re_a \to \infty$, y tends to the outer solution $y_o(x) = 2(1 + x)$ for $1 - x = \mathcal{O}(1)$ and to the inner solution $y_i(\eta) = 4\eta/(4 + \eta)$, $\eta = Re_a(1 - x)$ in the vicinity of $x = 1$. The inner solution describes the round Schlichting jet[6]; the outer solution describes a flow induced by a uniform sink along the axis $x = 1$ and $y_i(\infty) = y_o(1) = 4$.

Obtaining y_m and y_a, we find that y_m coincides with the exact solution y_e (for this particular example), whereas

$$y_a = y_e - 8(1 - x)/[4 + Re_a(1 - x)]$$

The error $y_e - y_a = 8(1 - x)/[4 + Re_a(1 - x)] < 8/Re_a$ uniformly tends to zero in $-1 \le x \le 1$ as $Re_a \to \infty$.

With the help of this asymptotic technique, we obtain composite solutions using Eq. (1) as an outer solution and matching it with appropriate inner solutions discussed next.

B. Inner Solutions

In particular, an inner solution is needed to make v_z bounded at $r = 0$. The inner solution must rapidly decay as r increases to match

the outer solution. This implies that v_z has its maximal value near the axis, with jet-like flow in the inner (core) region. The core radius is typically small in comparison to that of the outer region, where Eq. (1) is valid. For this reason, one can apply the boundary-layer approximation to the near-axis jet.

1. Long's Jet

A strong near-axis swirling jet is described by Long's[7] boundary-layer solution. Although Long's solution has no analytical representation, the asymptotic behavior of velocity can be written explicitly as[7]

$$v_r \to -\nu r^{-1} \tag{9a}$$

$$v_z \to \nu r^{-1}\Gamma/\sqrt{2} \tag{9b}$$

$$v_\phi \to \nu r^{-1}\Gamma \tag{9c}$$

as $r \to \infty$ at a fixed z. This asymptotic behavior is sufficient to show that Long's jet is well matched with Eq. (1). First, the asymptote for the swirl (9c) agrees with Eq. (1b). Note that the next term in the expansion[7] yields the difference $v_\phi - \nu r^{-1}\Gamma$, which vanishes exponentially as $r \to \infty$. This means that the agreement is excellent. Second, the asymptote for the radial velocity (9a) agrees with Eq. (1a) at $Re = -1$. Concerning the axial velocity, Eq. (9b) coincides with the third term of Eq. (1c) at $Re = -1$ and $W_r = \Gamma/\sqrt{2}$. We conclude that Long's jet is an appropriate inner solution and can be matched with Eq. (1) at $Re = -1$.

Note that the matching occurs for all velocity components. This is a favorable exception, as typically not all of the components can be matched to the leading order of magnitude. For example, the wall boundary-layer and outer solutions do not match with respect to the normal velocity v_y (whereas the longitudinal velocity v_x matches). Another example is the Landau jet, where the inner and outer solutions are matched in v_r but not in v_z. The exceptional matching of Long's jet and Eq. (1) occurs because v_r, v_z, and v_ϕ have the same asymptotic behavior ($\sim r^{-1}$ as $r \to \infty$) as given by Eq. (9).

It is striking that a more complicated near-axis jet does have an analytical solution as shown next.

2. Annular Jet

A sufficiently strong swirl induces inversion of the near-axis flow.[7] As the swirl increases, the position where the longitudinal velocity (at fixed z) is maximum shifts away from the axis. The axis is now the position of a local minimum of the longitudinal velocity. This minimum decreases as the swirl increases and then becomes negative ($v_z < 0$), i.e., flow reversal occurs. With a further increase in swirl, the $v_z < 0$ domain expands, and the reversed flow becomes irrotational. The near-axis region of the irrotational flow is bounded by an annular swirling jet.[2] Although the resulting flow pattern is rather complex, there are analytical solutions for large swirl, i.e., $\Gamma \gg 1$. One of the solutions[15] covers only a thin region along the axis, whereas the other[16] encompasses an outer (inviscid vortical) flow too. The solution[16] describes three flow regions.

1) Near-axis flow, $\psi_p = -\psi_s(1-x)/(1-x_j)$ and $v_\phi \equiv 0$ for $x_j < x \le 1$.

2) Annular jet, $\psi_j = -\psi_s \tanh\xi$ and $v_\phi = \Gamma\nu r^{-1}(1-\tanh\xi)/2$ in the vicinity of $x = x_j$.

3) Outer flow, $\psi_v = \psi_s\{x[2-(1+x_j)x/x_j]/[x_j(1-x_j)]\}^{1/2}$ and $v_\phi = \Gamma\nu r^{-1}$ for $0 \le x < x_j$.

Here

$$\psi_s = -\Gamma r_0^{-1} R x_j[(1-x_j)/(1+x_j)]^{\frac{1}{2}}$$

$$\xi = \Gamma x_j(x-x_j)\Big/\Big[2(1+x_j)\big(1-x_j^2\big)^{\frac{1}{2}}\Big], \qquad R = (r^2+z^2)^{\frac{1}{2}}$$

The annular jet direction is given by $x_j = \cos\theta_j$, with θ_j being the polar angle of the annular jet. The preceding solution can be combined into the composite solution

$$\psi = \psi_p(1+\tanh\xi)/2 + \psi_v(1-\tanh\xi)/2 \tag{10a}$$

$$v_\phi = \Gamma\nu r^{-1}(1-\tanh\xi)/2 \tag{10b}$$

which is a uniform approximation for the entire range $0 \le x \le 1$. A new control parameter introduced in Eq. (10) is x_j; the other parameters used are the same as in the outer solution (1). Considering x_j close to 1, i.e., small θ_j, we now match Eq. (10) with Eq. (1).

3. Strongly Swirling Composite Flow

First, we construct a bipolar jet flowing from the origin along the z axis in both directions. We start from solution (10), which is valid for $z > 0$ only. Denoting the stream function (10a) as ψ_+, we define $\psi_- = -\psi_+(-z)$ and introduce the combined inner solution $\psi_i = \psi_+$ for $z > 0$ and $\psi_i = \psi_-$ for $z < 0$. Thus, we obtain the inner solution ψ_i, which is an odd function of z and describes a bipolar jet. Smoothing of the inner solution near $z = 0$ and matching with the outer solution yields

$$\psi = a(r/r_0)^2 + \psi_i \tanh\big(d^2z^2/r_0^2\big) + c(r/r_0)^4 \tag{11a}$$

Because the swirl is symmetric with respect to $z = 0$, we have $v_{\phi i} = v_{\phi+}$ for $z > 0$ and $v_{\phi i} = v_{\phi-}$ for $z < 0$, where $v_{\phi+}$ is defined by Eq. (9a) and $v_{\phi-}(z) = v_{\phi+}(-z)$ for $z < 0$. Finally, regularization near the origin yields

$$v_\phi = v_{\phi i}\tanh\left[\frac{d^2(r^2+z^2)}{r_0^2}\right] \tag{11b}$$

The strongly swirling composite solution (11) models very complex flows having up to seven recirculatory zones[13] (depending on parameter values).

4. Weakly Swirling Composite Flow

As swirl decreases, the annular jet (10) first transforms into Long's jet and then to a weakly swirling jet, where the equations for the meridional flow become decoupled from that for the swirl. In this case, the meridional motion is described by the Schlichting solution[6]

$$v_z = \nu z^{-1} Re_a[1 + B(r/z)^2]^{-2} \tag{12a}$$

$$v_r = 4\nu B r z^{-2}[1 - B(r/z)^2]/[1 + B(r/z)^2]^2 \tag{12b}$$

$$\psi = -Br^2(zr_0)^{-1}[1 + B(r/z)^2]^{-1} \tag{12c}$$

where Re_a is the dimensionless velocity on the axis and $B = Re_a/8 = 3J(64\pi\rho\nu^2)^{-1}$, with J the axial momentum flux through a plane normal to the jet axis.

For a fixed z, Eq. (12b) indicates that $v_r \to -4\nu r^{-1}$ as $r \to \infty$. This exactly coincides with Eq. (1a) at $Re = -4$. The asymptotic relation for the axial velocity is $v_z \to 8\nu B^{-1}z^3r^{-4}$ (as $r \to \infty$) according to Eq. (12a). Thus, v_z has the same power with respect to r as Eq. (1c) at $W_c = W_p = 0$, $Re = -4$. Note that the Schlichting jet and Eq. (1) are matched with respect to v_r but not with v_z, like the Landau jet (Sec. VI.A).

The boundary-layer solution for the weak swirl is[1]

$$v_\phi = \Gamma\nu r^{-1}[1 + z^2/(Br^2)]^{-1} \tag{12d}$$

The asymptotic expansion of Eq. (12d) as $r \to \infty$ at a fixed z is

$$v_\phi = \Gamma\nu r^{-1} - \Gamma\nu B^{-1}z^2r^{-3} + \cdots$$

Therefore, Eq. (12d) is an appropriate inner solution for matching with Eq. (1b).

The additive composite solution is

$$\psi = a(r/r_0)^2 - 1\Big/\big\{Br^2(zr_0)[1+B(r/z)^2]\big\}\tanh\big(z^2d^2/r_0^2\big) + c(r/r_0)^4 \tag{13a}$$

$$v_\phi = \Gamma\nu r^{-1}[1 + z^2/(Br^2)]^{-1}\tanh\big[(r^2+z^2)d^2/r_0^2\big] \tag{13b}$$

The factors $\tanh(z^2d^2/r_0^2)$ and $\tanh[(r^2+z^2)d^2/r_0^2]$ are used here to smooth the singularity at $z = 0$, and the parameter d defines the smoothing scale r_0/d. The value of d has minor influence on the global flow pattern.

The typical flow patterns, i.e., streamlines of the meridional motion and the corresponding profile of $v_z(r)$ at $z = -\infty$, described by Eq. (13a) are presented in Ref. 17. The composite solution models complex meridional flows. These flows result from contributions due to the uniform stream, axial pressure gradient, and radial flow induced by the swirl.

Thus, solution (13) describes a variety of flow patterns, which typically occur in vortex devices. Now we apply this solution to model the flowfield and the flame front in a vortex burner.

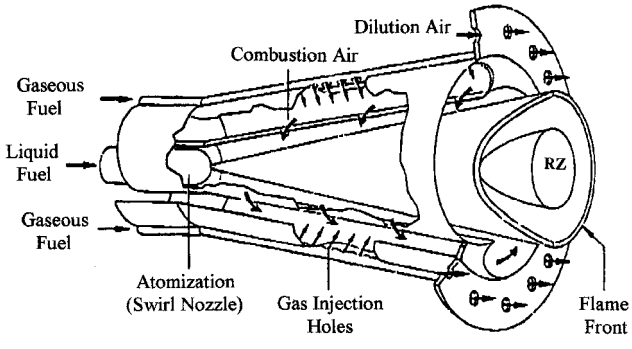

Fig. 4a Schematic of the ABB burner.[19]

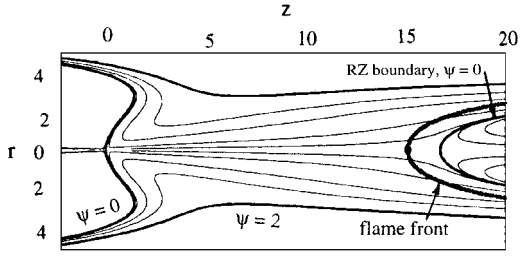

Fig. 4b Our model of the meridional flow and flame front.

VII. Vortex Burner

A. Flowfield

It is well known that swirling flows with recirculatory zones provide flame stabilization and are favorable for combustion.[18] Figure 4a shows a schematic of a burner of the ABB Power Generation Gas Turbine.[19] Tangential injection of gaseous fuel and air through the slits in the conical sidewall generates a strongly swirling flow inside the burner. Liquid fuel, injected through the central nozzle, is atomized into drops and evaporated. The recirculatory zone (RZ) (see the near-axis parabolic region close to the exit) provides the upstream location of the stabilized flame front (shown as a double parabolic curve in Fig. 4a).

Figure 4b shows a flow pattern obtained with the help of the matched solution (13) for $a = -0.33$, $B = 5$, $c = 0.02$, and $d = 5$. Taking into account the turbulent character of the flow in the burner, we interpret ν as the eddy viscosity, disregard the no-slip condition, and replace some of the streamlines by walls, as shown in Fig. 4b. Hence, we cannot expect that this solution gives an accurate representation of the practical flow. However, our solution describes important qualitative properties of the flow, as comparison of Figs. 1a and 1b shows. The streamlines $\psi = 2$ shown by a bold curve in Fig. 4b serve as the burner sidewall. The bold curve $\psi = 0$ in the left part of Fig. 2b imitates the endwall; the other bold curve $\psi = 0$ located near the exit represents the boundary of the recirculatory zone. There are also streamlines $\psi = -0.025$ and -0.05 inside and $\psi = 0.01, 0.1, 0.5$, and 1 outside the RZ.

B. Model for the Flame Front

To model the flame front, we apply the following approach. Consider the contribution to heat and mass transfer from diffusion to be small in comparison with that from advection. Also neglect the thickness of the flame front and treat the front as a surface having uniform temperature and concentration (ignition values). Then for steady fronts, the normal-to-front velocity of the flow v_n is also uniform and equals $-v_c$, where v_c is the propagation speed of combustion. Therefore, in such an approach,[20,21] the flame front is a surface $F(r, z) = 0$ governed by the equation[22]

$$v_r \frac{\partial F}{\partial r} + v_z \frac{\partial F}{\partial z} = -v_c \left[\left(\frac{\partial F}{\partial r} \right)^2 + \left(\frac{\partial F}{\partial z} \right)^2 \right]^{\frac{1}{2}} \tag{14a}$$

Representing $F \equiv z - Z(r)$ and substituting in Eq. (14a) yields

$$\frac{\mathrm{d}Z}{\mathrm{d}r} = \left[v_c \left(v_r^2 + v_z^2 - v_c^2 \right)^{\frac{1}{2}} - v_r v_z \right] \Big/ \left(v_c^2 - v_r^2 \right) \tag{14b}$$

The flame front calculated with the help of Eq. (14) is shown by the bold curve slightly upstream of the RZ. The flame propagates upstream (to the region where there is unburned fuel) and the advection velocity must be positive to make the front stagnant. The choice of v_c depends on combustion components, e.g., for combustion of pure methane in air, $v_c = 0.3$ m/s, which is the marginal value of self-ignition.[22]

VIII. Conclusion

1) The obtained exact solution (1) and composite solutions (10) and (13) allow modeling complex swirling flows.

2) The new solutions of the heat and diffusion equations (Secs. III–V) describe a variety of axisymmetric and three-dimensional fields of temperature and concentration.

3) These solutions are applied to model a vortex burner.

4) The analytical nature of these solutions permits a wide parametric study to optimize the vortex burner geometry, the flowfield, and the flame front.

Acknowledgment

This research was funded by National Science Foundation Grant CTS-9622302.

References

[1]Goldshtik, M. A., and Shtern, V. N., "Collapse in Conical Viscous Flows," *Journal of Fluid Mechanics*, Vol. 218, Sept. 1990, pp. 483–508.

[2]Shtern, V., and Hussain, F., "Hysteresis in Swirling Jets," *Journal of Fluid Mechanics*, Vol. 309, Feb. 1996, pp. 1–44.

[3]Borissov, A. A., Kuibin, P. A., and Okulov, V. L., "Calculation of the Ranque Effect in the Vortex Tube," *Acta Mechanica*, Vol. 4, Supplement, 1994, pp. 289–295.

[4]Saffman, P. G., *Vortex Dynamics*, Cambridge Univ. Press, Cambridge, England, UK, 1992, Chap. 7.

[5]Wang, C. Y., "Exact Solutions of the Steady-State Navier–Stokes Equations," *Annual Review of Fluid Mechanics*, Vol. 23, 1991, pp. 159–177.

[6]Schlichting, H., *Boundary-Layer Theory*, 6th ed., McGraw–Hill, New York, 1979, pp. 218–222.

[7]Long, R. R., "A Vortex in an Infinite Viscous Fluid," *Journal of Fluid Mechanics*, Vol. 11, Pt. 4, 1961, pp. 611–623.

[8]Fulton, C. D., "Ranque Tube," *Refrigeration Engineering*, Vol. 58, No. 5, 1950, pp. 473–479.

[9]Sarpkaya, T., "Vortex Breakdown in Conical Swirling Flows," *AIAA Journal*, Vol. 9, No. 9, 1971, pp. 1792–1799.

[10]Serrin, J., "The Swirling Vortex," *Philosophical Transactions of the Royal Society of London*, Vol. A271, No. 1274, 1972, pp. 325–360.

[11]Burrgraf, O. R., and Foster, M. R., "Continuation or Breakdown in Tornado-Like Vortices," *Journal of Fluid Mechanics*, Vol. 80, Pt. 4, 1977, pp. 685–704.

[12]Batchelor, G. K., *An Introduction to Fluid Dynamics*, Cambridge Univ. Press, Cambridge, England, UK, 1967, pp. 602, 603.

[13]Borissov, A., Shtern, V., and Hussain, F., "Analytical Models for Complex Swirling Flows," *Bulletin of the American Physical Society*, Vol. 41, No. 9, 1996, p. 1787.

[14]Van Dyke, M., *Perturbation Methods in Fluid Mechanics*, Academic, New York, 1964, pp. 94–96.

[15]Foster, M. R., and Smith, F. T., "Stability of Long's Vortex at Large Flow Force," *Journal of Fluid Mechanics*, Vol. 206, Sept. 1989, pp. 405–452.

[16]Shtern, V., and Hussain, F., "Hysteresis in a Swirling Jet as a Model Tornado," *Physics of Fluids*, Vol. 5, No. 9, 1993, pp. 2183–2195.

[17]Shtern, V., Borissov, A., and Hussain, F., "Vortex-Sinks with Axial Flow: Solution and Applications," *Physics of Fluids*, Vol. 9, No. 10, 1997, pp. 2941–2959.

[18]Gupta, A. K., Lilley, D. G., and Syred, N., *Swirl Flows*, Abacus, Tunbridge Wells, England, UK, 1984, Chap. 1.

[19]Keller, J. J., Sattelmayer, T., and Thuringer, F., "Double-Cone Burner for Gas Turbine Type 9 Retrofit Application," *Proceedings of the 19th International Congress on Combustion Engines* (Florence, Italy), 1991.

[20]Markstein, G. H., *Unsteady Flame Propagation*, Pergamon, Oxford, England, UK, 1964, p. 8.

[21]Williams, F. A., *Combustion Theory*, 2nd ed., Addison–Wesley, Reading, MA, 1984, p. 44.

[22]Borisov, A. A., Kuibin, P. A., and Okulov, V. L., "Flame Shapes in Swirl Flows," *Russian Journal of Engineering Thermophysics*, Vol. 3, No. 2, 1993, pp. 243–255.

J. Kallinderis
Associate Editor